A Direct Torque Vector Neural Control of a Three Phase Induction Motor

Ieroham S. Baruch, Carlos-Roman Mariaca G., and Irving-Pavel de la Cruz A.
CINVESTAV-IPN, Department of Automatic Control, Av. IPN No 2508, Col. Zacatenco, A.P. 14-740, 07360 Mexico D.F., Mexico
{baruch, cmariaca}@ctrl.cinvestav.mx

(Paper received on August 11, 2006, accepted on September 26, 2006)

Abstract. The paper proposed a neural solution to the direct torque vector control of three phase induction motor including real-time trained recurrent neural velocity controller and a hysteresis flux and torque controllers, which permitted the speed up reaction to the variable load. The basic equations and elements of the direct field oriented torque control scheme are given. The control scheme is realized by one RNN learned by a real-time BP algorithm and three FFNNs learned off-line by Levenberg-Marquardt algorithm with data taken from PI-control scheme simulations. The graphical results of modelling shows a better performance of the NN control system with respect to the PI controlled system realizing the same general control scheme.

1. Introduction

The Neural Networks (NN) applications for identification and control of electrical drives became very popular in last decade. In [1], a multilayer-perceptron-based-neural-control is applied for a DC motor drive. In [2], a recurrent neural network is applied for identification and adaptive control of a DC motor drive mechanical system. In the last decade a great boost is made in the area of induction motor drive control. The induction machine, particularly the cage type, is most commonly used in adjustable speed AC drive systems [3]. The control of AC machines is considerably more complex than that of DC machines. The complexity arises because of the variable-frequency power supply, AC signals processing, and complex dynamics of the AC machine [3], [4]. In the vector or Field-Oriented Control (FOC) methods, an AC machine is controlled like a separately excited DC machine, where the active (torque) and the reactive (field) current components are orthogonal and mutually decoupled so they could be controlled independently, [3]-[6]. There exist two methods for PWM current controlled inverter – direct and indirect vector control, [3]. This paper considered the direct control method, where direct AC motor measurements are used for field orientation and control. There are several papers of NN application for AC motor drive direct vector control. In [7] a Feedforward NN (FFNN) is used for vector PW modulation, resulting in a faster response. In [8] an Artificial NN is used for fast estimation of the angle used in a FOC system. Some basic principles of the direct torque control of IM drives are given in [9]. The [10] applied NNs in the direct torque control of IM drive. In [11], a FFNN is used for commutation table emulation in a direct torque control of IM. In [12], the authors proposed to use a NN so to compensate the variations of the

Special Issue in Neural Networks and Associative Memories
Research in Computing Science 21, 2006, pp. 131-140

stator resistance, necessary for the FOC of flux in a direct torque IM control scheme. In [13] off-line trained FFNNs-are used to substitute the blocks of coordinate transformation, vector flux computation, torque estimation, and commutations table realization in a direct self-tuning IM control scheme. In [14] a FFNN-based estimator of the feedback signals is used for induction motor drive direct FOC system. The paper [15] proposed two NN-based methods (direct and indirect) for FOC of induction motors. The results and particular solutions obtained in the referenced papers shows that the application of NN offers a fast and improved alternative of the classical FOC schemes. The present paper proposed a neural solution of a direct torque vector control problem that assures fast response and adaptation to a variable load.

2. Mathematical Models of the Three Phase Induction Motor

A Phase (a, b, c) Model: The Induction Motor (IM) equations, [5], [6], for stator and rotor voltages in vector-matrix form are given as:

$$\mathbf{v}_{abcs} = \mathbf{r}_s \mathbf{i}_{abcs} + p\boldsymbol{\lambda}_{abcs}; \mathbf{v}_{abcr} = \mathbf{r}_r \mathbf{i}_{abcr} + p\boldsymbol{\lambda}_{abcr}; \mathbf{r}_s = r_s \mathbf{I}_3; \mathbf{r}_r = r_r \mathbf{I}_3 \tag{1}$$

$$\begin{aligned} &\mathbf{v}_{abcs} = (v_{as}, v_{bs}, v_{cs})^T; \mathbf{v}_{abcr} = (v_{ar}, v_{br}, v_{cr})^T \\ &\mathbf{i}_{abcs} = (i_{as}, i_{bs}, i_{cs})^T; \mathbf{i}_{abcr} = (i_{ar}, i_{br}, i_{cr})^T \\ &\boldsymbol{\lambda}_{abcs} = (\lambda_{as}, \lambda_{bs}, \lambda_{cs})^T; \boldsymbol{\lambda}_{abcr} = (\lambda_{ar}, \lambda_{br}, \lambda_{cr})^T \end{aligned} \tag{2}$$

Where the variables are: voltage, current, and flux, stator and rotor, three dimensional (a, b, c) vectors, with given up phase components; $\mathbf{r}_s$ and $\mathbf{r}_r$ are stator and rotor winding resistance diagonal matrices, with given up equal elements r_s and r_r, respectively; $\mathbf{I}_3$ is an identity matrix with dimension three, and p is a Laplacian differential operator. The vector-matrix block-form representation of the flux leakage is given by the equation:

$$\begin{bmatrix} \boldsymbol{\lambda}_{abcs} \\ \boldsymbol{\lambda}_{abcr}^{'} \end{bmatrix} = \begin{bmatrix} \mathbf{L}_{ss}^{abc} & \mathbf{L}_{sr}^{'abc} \\ (\mathbf{L}_{sr}^{'abc})^T & \mathbf{L}_{rr}^{'abc} \end{bmatrix} \begin{bmatrix} \mathbf{i}_{abcs} \\ \mathbf{i}_{abcr}^{'} \end{bmatrix} \tag{3}$$

Where: the stator, rotor and mutual block-inductance (3x3) matrices are described in [5], [6]. The relative leakage inductance depends on the winding turn stator/rotor ratio n, and on the angular rotor position $_r$ respectively [5], [6]. Finally, the voltage equations (1) could be expressed with respect to the stator in the (a, b, c) model form:

$$\begin{bmatrix} \mathbf{v}_{abcs} \\ \mathbf{v}_{abcr}^{'} \end{bmatrix} = \begin{bmatrix} \mathbf{r}_s + p\mathbf{L}_{ss}^{abc} & p\mathbf{L}_{sr}^{'abc} \\ (p\mathbf{L}_{sr}^{'abc})^T & \mathbf{r}_r + p\mathbf{L}_{rr}^{'abc} \end{bmatrix} \begin{bmatrix} \mathbf{i}_{abcs} \\ \mathbf{i}_{abcr}^{'} \end{bmatrix}; \begin{aligned} &\mathbf{v}_{abcr}^{'} = n\mathbf{v}_{abcr}; \mathbf{i}_{abcr}^{'} = (1/n)\mathbf{i}_{abcr} \\ &\boldsymbol{\lambda}_{abcr}^{'} = n\boldsymbol{\lambda}_{abcr}; \mathbf{r}_r^{'} = n^2 \mathbf{r}_r \end{aligned} \tag{4}$$

Where the given up variables are the relative rotor voltage, the current, the flux and the resistance.

A (q, d, 0) Model: The (a, b, c) model is very complicated for control, so it could be simplified using a transformation to the (q, d, 0) form. The AC motor equations for the stator and rotor voltages in (q, d, 0) vector-matrix form are given as follows:

$$\mathbf{v}_{qd0s} = \mathbf{r}_s \mathbf{i}_{qd0s} + \Omega\boldsymbol{\lambda}_{qd0s} + p\boldsymbol{\lambda}_{qd0s}\,;\; \mathbf{v}'_{qd0r} = \mathbf{r}_r \mathbf{i}'_{qd0r} + \Delta\Omega\boldsymbol{\lambda}'_{qd0r} + p\boldsymbol{\lambda}'_{qd0r} \tag{5}$$

$$\begin{aligned}
&\mathbf{v}_{qd0s} = \left(v_{qs}, v_{ds}, v_{0s}\right)^T ; \mathbf{v}'_{qd0r} = \left(v'_{qr}, v'_{dr}, v'_{0r}\right)^T \\
&\mathbf{i}_{qd0s} = \left(i_{qs}, i_{ds}, i_{0s}\right)^T ; \mathbf{i}'_{qd0r} = \left(i'_{qr}, i'_{dr}, i'_{0r}\right)^T \\
&\boldsymbol{\lambda}_{qd0s} = \left(\lambda_{qs}, \lambda_{ds}, \lambda_{0s}\right)^T ; \boldsymbol{\lambda}'_{qd0r} = \left(\lambda'_{qr}, \lambda'_{dr}, \lambda'_{0r}\right)^T
\end{aligned} \tag{6}$$

Where the variables are: voltage, current, and flux, stator and rotor, three dimensional vectors, with given up components; $\mathbf{r}_s$ and $\mathbf{r}_r$ are stator and rotor resistance diagonal matrices, given by (1); , and are diagonal angular velocity matrices, given by:

$$\Omega = \begin{bmatrix} \omega & 0 & 0 \\ 0 & -\omega & 0 \\ 0 & 0 & 0 \end{bmatrix}; \Delta\Omega = \begin{bmatrix} \omega - \omega_r & 0 & 0 \\ 0 & -(\omega - \omega_r) & 0 \\ 0 & 0 & 0 \end{bmatrix} \tag{7}$$

The vector-matrix block-form representation of the flux leakage is given by:

$$\begin{bmatrix} \boldsymbol{\lambda}_{qd0s} \\ \boldsymbol{\lambda}'_{qd0r} \end{bmatrix} = \begin{bmatrix} \mathbf{L}_{ss}^{qd0} & \mathbf{L}_{sr}^{qd0} \\ (\mathbf{L}_{sr}^{qd0})^T & \mathbf{L}_{rr}^{qd0} \end{bmatrix} \begin{bmatrix} \mathbf{i}_{qd0s} \\ \mathbf{i}'_{qd0r} \end{bmatrix} \tag{8}$$

Where: the stator, rotor and mutual block-inductance (3x3) matrices are given in [5], [6]. The (q, d, 0) model could be written in the stationary and synchronous frames taking the angular velocity equal to: =0 and = $_e$ where $_e$, corresponds to the angular velocity of the stator field. Now we could write the scalar electromagnetic torque equation that could be expressed in the following basic forms used:

$$\begin{aligned}
&T_{em} = \frac{3}{2}\frac{P}{2}\boldsymbol{\lambda}'^{T}_{q-d,r}\mathbf{i}'_{d-q,r} = \frac{3}{2}\frac{P}{2}\mathbf{i}'^{T}_{d-q,r}\mathbf{i}_{q-d,s}\,; \\
&\mathbf{i}_{q-d,s} = \left(i_{qs}, i_{ds}\right)^T ; \mathbf{i}'_{d-q,r} = \left(i'_{dr}, -i'_{qr}\right)^T ; \boldsymbol{\lambda}'_{q-d,r} = \left(\lambda'_{qr}, \lambda'_{dr}\right)^T
\end{aligned} \tag{9}$$

where: P is a number of poles.

Field Orientation Conditions: The flux and torque equations decoupling needs to transform the stator flux, current and voltage vectors from (a, b, c) reference frame into (q-d,s) reference frame and than to stationary and synchronous reference frames, [6]. The Fig. 1a illustrates the current and voltage vector representations in stator and rotor synchronous frames and also the magnetic field orientation, where the rotor flux vector is equal to the d-component of the flux vector, represented in a synchronous reference

frame ($'^{e}_{dr} = {}_{r}$), which is aligned with the d-component of the current in this frame. For more clarity, the current and flux orientation in the synchronous reference frame are shown on Fig. 1b. So, the field orientation conditions are:

$$\lambda'^{e}_{qr} = 0; p\lambda'^{e}_{qr} = 0; \lambda_r = \lambda'^{e}_{dr} \tag{10}$$

Taking into account that the rotor windings are shortcut, (the rotor voltage is zero) and the given up field orientation conditions the first two components of (5) become:

$$0 = r'_r i'^{e}_{qr} + (\omega_e - \omega_r)\lambda'^{e}_{dr}; 0 = r'_r i'^{e}_{dr} + p\lambda'^{e}_{dr} \tag{11}$$

From (5), for the q-component of the rotor flux, it is obtained:

$$\lambda'^{e}_{qr} = L_m i^{e}_{qs} + L'_r i'^{e}_{qr} = 0; L'_r = L'_{lr} + L_m; i'^{e}_{qr} = -(L_m / L'_r) i^{e}_{qs}; \tag{12}$$

Taking into account (10) and (12), the torque equation (9) obtained the final form:

$$T_{em} = \frac{3}{2}\frac{P}{2}\frac{L_m}{L'_r}\lambda'^{e}_{dr} i^{e}_{qs} \tag{13}$$

The equation (13) shows that if the flux of the rotor is maintained constant, so the torque could be controlled by the q-component of the stator current in synchronous reference frame. From the second equation of (11), taking into account (12) it is easy to obtain the slipping angular velocity as:

$$\omega_e - \omega_r = (r'_r L_m / L'_r)(i^{e}_{qs} / \lambda'^{e}_{dr}) \tag{14}$$

The final equations (12), (13), (14) gives us the necessary basis for a direct decoupled field oriented (vector) control of the AC motor drive, where following Fig. 1(b), the q-component of the stator current produced torque and the d-component of the stator current produced flux.

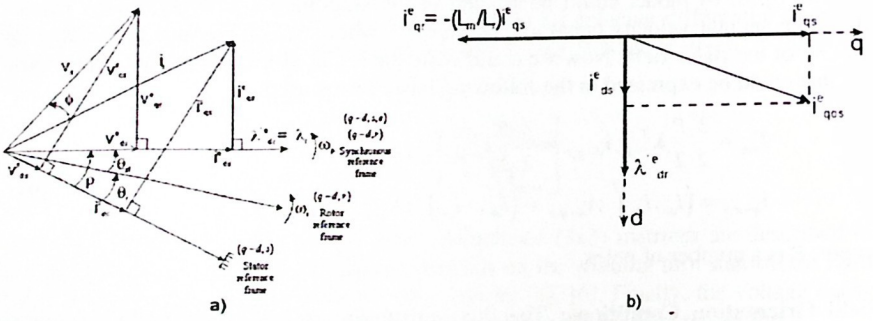

Fig. 1. Vector diagrams of the stator current, voltage and the rotor flux. a) The current and voltage vector representations in stator and in rotor synchronous reference frames. b) The stator current and the rotor flux vector representations in synchronous reference frame.

Coordinate Transformations: The combined stator current transformation from (a, b, c) to (q-d,s,e) synchronous reference frame [5], [6], is given by the equation:

$$\begin{bmatrix} i^e_{qs} \\ i^e_{ds} \end{bmatrix} = \begin{bmatrix} \cos\rho & f_1 & f_2 \\ sin\rho & f_3 & f_4 \end{bmatrix} \begin{bmatrix} i_{as} \\ i_{bs} \\ i_{cs} \end{bmatrix}; \quad \begin{aligned} f_1 &= [-(1/2)\cos\rho - (\sqrt{3}/2)sin\rho] \\ f_2 &= [-(1/2)\cos\rho + (\sqrt{3}/2)sin\rho] \\ f_3 &= [-(1/2)sin\rho + (\sqrt{3}/2)\cos\rho] \\ f_4 &= [-(1/2)sin\rho - (\sqrt{3}/2)\cos\rho] \end{aligned} \tag{15}$$

Flux and Torque Estimation: From the equation (5), written for the stationary reference frame (=0), we could obtain:

$$\lambda^s_{qs} = (1/p)\left(v^s_{qs} - r_s i^s_{qs}\right); \lambda^s_{ds} = (1/p)\left(v^s_{ds} - r_s i^s_{ds}\right) \tag{16}$$

The stator flux part of the equation (8) could be resolved for the rotor currents, as it is:

$$i^{'s}_{qr} = (\lambda^s_{qs} - L_s i^s_{qs})/L_m; i^{'s}_{dr} = (\lambda^s_{ds} - L_s i^s_{ds})/L_m \tag{17}$$

Substituting (17) back in the rotor flux part of (8) we could obtain:

$$\lambda^{'s}_{qr} = (L'_r/L_m)\left(\lambda^s_{qs} - L'_s i^s_{qs}\right); \lambda^{'s}_{dr} = (L'_r/L_m)\left(\lambda^s_{ds} - L'_s i^s_{ds}\right); L'_s = [L_s - (L^2_m/L'_r)] \tag{18}$$

Now it is easy to compute the angle needed for field orientation, the rotor flux, and the sin, cos - functions of this angle, needed for flux control, torque estimation, and coordinate transformations, which is:

$$\begin{aligned} &\lambda'_r = \sqrt{(\lambda^{'s}_{qr})^2 + (\lambda^{'s}_{dr})^2}; \rho = \tan^{-1}(\lambda^{'s}_{qr}/\lambda^{'s}_{dr}); \\ &sin\rho = \lambda^{'s}_{qr}/\lambda'_r; \cos\rho = \lambda^{'s}_{dr}/\lambda'_r \end{aligned} \tag{19}$$

The torque equation (13) could be rewritten in the form:

$$T_{em} = \frac{3}{2}\frac{P}{2}\frac{L_m}{L'_r}\lambda'_r i^e_{qs} \tag{20}$$

3. Direct Torque vector Control of the Induction Motor

A General Control Scheme: A general block diagram of the direct torque vector control of the Induction Motor drive is given on Fig. 2(a). The direct torque control scheme contains three principal blocks. They are: G1 – block of a velocity PI controller; G2, G3 –blocks of hysteresis flux and torque controllers; B1 – block of angle (N) computation; block of voltage commutations look up table; block of coordinate (a, b, c) to (q-d, s, e) transformation (see equation. (15)); block of a vector estimation, performing the field orientation, i.e. the torque, the flux and the angle- -computations, see equations (30), (31); block of the IM converter-machine system. The block of the IM

converter machine system contains a three phase bridge ASCI DC-AC voltage fed inverter, an induction motor model, and a model of the whole mechanical system driven by the IM ((2/P)J(d ω/dt)=T_{em}-T_L, where J is the moment of inertia, T_L is the load torque). The block of vector estimation performed rather complicated computations, so it contains various blocks, illustrated by Figs. 2(b) and 2(c). Fig. 2(b) illustrates the flux and angle estimation for field orientation, computing (16), (18), (19). The rotor flux computations block (see Fig. 2(b)) performs computations given by (16), (18), illustrated by Fig. 2(c). The direct torque control is effectuated through a look up table of voltage commutations that determine the on-off position of the thyristors in three phase bridge inverter. The table entries are the torque and flux errors and the stator field angle. The torque and flux errors are discretized in 60° phase angle by hysteresis comparators of two and three levels, respectively.

A Neural Networks Realization of the Control Scheme: The simplified Block-Diagram (BD) of the indirect neural vector control system, given on Fig. 3 is partly realized by four NNs, which function, topology and learning are briefly described.

The first Recurrent NN1 (RNN1) is an angular velocity recurrent neural controller with one input (the velocity error), one output (the torque set point), where the To = 0.01 sec. is chosen with respect to the stator electrical time constant. The weights learning is done in real – time using the Backpropagation (BP) algorithm. The RNN topology and learning are described in [2]. The RNN1 function is given by:

$$T^*(k+1) = \varphi\{c(k+1)\cdot\varphi[-a(k)x(k)+b(k)e_{vel}(k)-w^h(k)]-w^o(k+1)\} \qquad (21)$$

Where: a(.) and b(.) are hidden layer RNN1 weights; c(.) is an output layer RNN1 weight; w^h(.), w^o(.) are threshold weights of the hidden and output RNN1 layers, respectively; is a tanh activation function; e_{vel} is a velocity error; T* is the torque set point – output of the RNN1. The BP algorithm of learning for the output layer of the RNN1, [2], is given by:

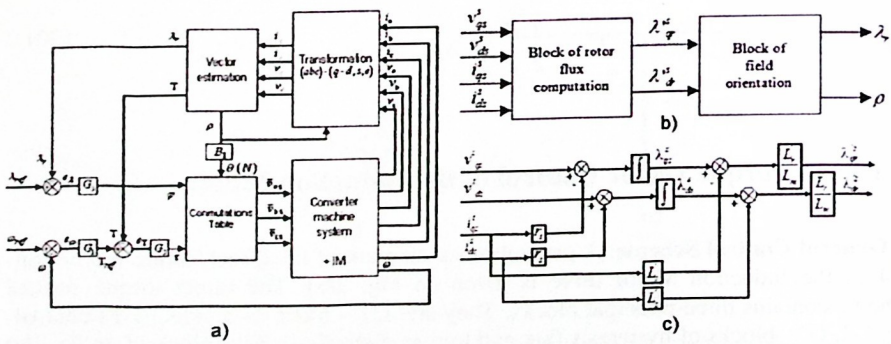

Fig. 2. Block diagrams. a) General BD of a direct IM vector control. b) BD of the vector estimation computations. c) BD of the flux estimation computations.

$$c(k+1) = c(k) + \eta e_{wf}(k)[1-(T^*(k))^2]z(k); \qquad (22)$$
$$w^n(k+1) = w^n(k) + \eta e_{wf}(k)[1-(T^*(k))^2](-1)$$

The BP algorithm of learning for the hidden layer of the RNN1, [2], is given by:

$$a(k+1) = a(k) + \eta R(k)x(k); b(k+1) = b(k) + \eta R(k)e_{wf}(k) \qquad (23)$$
$$w^h(k+1) = w^h(k) + \eta R(k)(-1); R(k) = c(k)e_{wf}(k)[1-(z(k))^2]$$

Where the learning rate is: =0.01.

The second Feedforward NN2 performed the rotor torque estimation (see equation (20)). The rotor (q-d,r) flux components $^{s}_{qs}$, $^{s}_{ds}$ are previously computed using equation (16) (see Fig.2c), and they are inputs of FFNN2. The other two inputs are the stator current components- i^{s}_{qs}, i^{s}_{ds}. The FFNN2 output is the torque- T_{em}. The FFNN2 topology is (4-20-5-1). The FFNN2 learning is off-line, applying the Levenberg-Marquardt (L-M) algorithm [16], [17]. The final value of the MSE reached is of 10^{-10}. The FFNN2 is learned and generalized by 2500 input-output patterns in 1179 epochs.

The third Feedforward NN3 performed rotor flux estimation using (19) equation. The rotor (q-d,r) flux components- $^{s}_{qs}$, $^{s}_{ds}$ are previously computed using equation (16) (see Fig.2c), and they are inputs of FFNN3. The FFNN3 output is the rotor flux- $_{r}$. The FFNN3 topology is (2-20-5-1). The FFNN3 learning is off-line, applying the L-M algorithm. The final value of the MSE reached is of 10^{-10}. The FFNN3 is learned and generalized by 2500 input-output patterns in 617 epochs.

The fourth Feedforward NN4 performed rotor flux estimation using (19) equation. The rotor (q-d,r) flux components- $^{s}_{qs}$, $^{s}_{ds}$ are previously computed using equation (16) (see Fig. 2©), and they are inputs of FFNN4. The FFNN4 output is the field angle . The FFNN4 topology is (2-20-5-1). The FFNN4 learning is off-line, applying the L-M algorithm. The final value of the MSE reached is of 10^{-10}. The FFNN4 is learned and generalized by 2500 input-output patterns in 727 epochs.

4. Graphical Results of the Control System Modeling

The parameters of the IM used in the control system modelling are: power- 20Hp; nominal velocity – N=1800 Rev.pm; pole number P = 4; voltage- 220 volts; nominal current – 75 A; phase number 3; nominal frequency 60 Hz; stator resistance r_s = 0,1062 Ohms; rotor resistance referenced to stator r_r'= 0.0764 Ohms; stator inductance L_s = 0.5689. 10^{-3} Henry; rotor inductance referenced to stator L_r' = 0.5689. 10^{-3} Henry; magnetizing inductance L_m = 15.4749. 10^{-3} Henry; moment of inertia J = 2.8 kg.m^2. The control system modeling is done changing the load torque in different moment of time. Figs. 3 (a) and 3 (b) show the angular velocity set point vs. the IM angular velocity in the general case of velocity control and particularly with load torque changes. The results show that the angular velocity control system has a fast speed up response and satisfactory behaviour in the case of load change. Figs. 4(a) and 4 (b) show the flux graphics of control system with hysteresis control applying the classical control scheme and applying the scheme using NNs. The results show a faster and better re-

sponse of the neural system. Figs. 5(a) and 5(b), Figs. 6(a) and 6(b) show the torque graphics with hysteresis control in the same cases and a load changes. The results show a faster and better response of the neural system. Figs. 7(a) and 7(b) and Figs. 7(c) and 7(d) shows the (a,b,c) stator currents of hysteresis controlled system using classical and neural control schemes in load changes conditions for different time intervals. The results show a good performance of the neural control system at all.

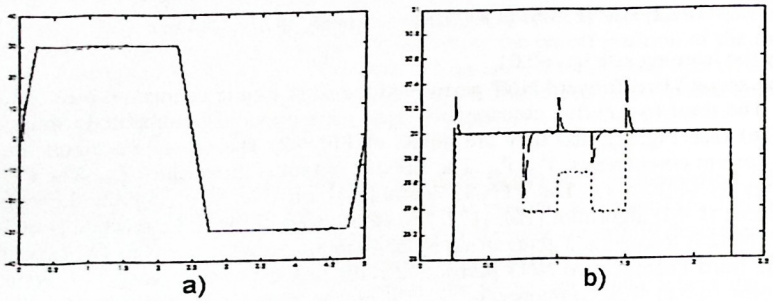

Fig. 3. Graphical results of the IM velocity control. a) General graphics of the angular velocity control; b) Graphical results of angular velocity control with load changes.

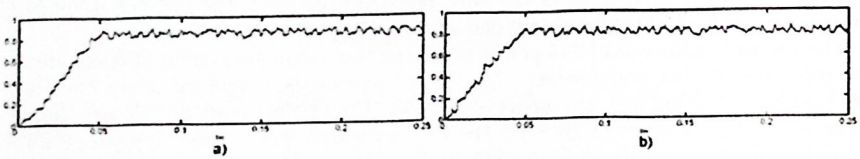

Fig. 4. Graphical results of the IM flux control. a) Graphics of the flux classical control; b) Graphics of the flux control using neural networks.

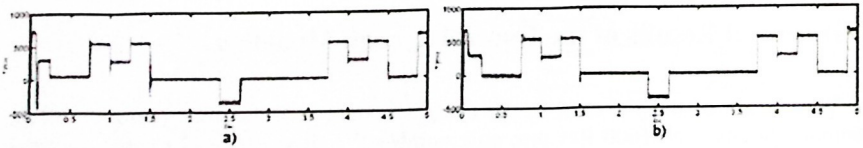

Fig. 5. Graphics of the process history of the torque control with load changes. a) Graphics of the torque classical control. b) Graphics of the torque control using neural networks.

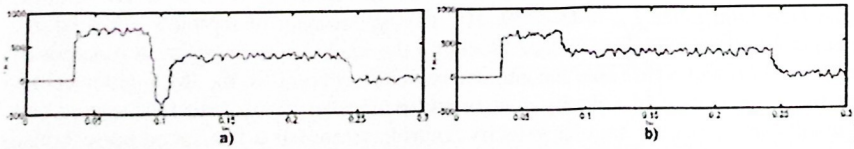

g. 6. Detailed graphics of the torque control using both control schemes and load changes. a) Classical control; b) Control using neural networks.

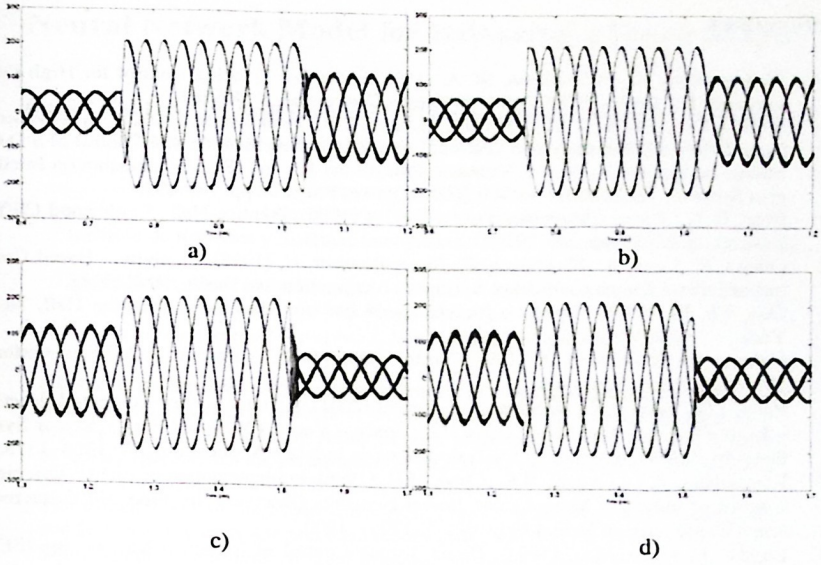

Fig. 7. Graphical results of (a,b,c) stator currents during load changes. a) and c) Classical control. b) and d) Control using neural networks.

5. Conclusions

The paper proposed a neural network solution to the direct torque vector control of a three-phase induction motor including velocity RNN controller, and hysteresis controllers for flux and torque, which permitted the speed up reaction to the variable load. The period of discretization of the RNN velocity controller is chosen with respect to the AC stator electrical time constant. The basic equations and elements of the direct field oriented torque control scheme are given. The control scheme is realized by one RNN BP real-time velocity controller and three FFNN learned off-line by Levenberg-Marquardt algorithm with data taken by classical control simulations. The LM algorithm has a 10^{-10} set up error precision. The graphical simulation results exhibited a better performance of the adaptive NN control system with respect to the classical control in variable load conditions.

Acknowledgements

We want to thank CONACYT, Mexico for the scholarships given to PhD student Carlos Roman Mariaca Gaspar and MS student Irving Pavel de la Cruz Arguello, during his studies in CINVESTAV-IPN, Mexico.

References

[1] Weerasooriya, S., El-Sharkawi, M. A. (1991): Adaptive Tracking Control for High Performance DC Drives. IEEE Trans. on Energy Conversion, 4:182-201.

[2] Baruch, I. S., Flores, J. M., Nava, F., Ramirez, I. R., Nenkova, B. (2002). An Advanced Neural Network Topology and Learning, Applied for Identification and Control of a D.C. Motor. In: Sgurev, V., Jotsov, V. (eds.): Proc. of the 1-st Int. IEEE Symposium on Intelligent Systems. IEEE, ISBN 0-7803-7601-3, Varna, Bulgaria, pp. 289-295.

[3] Bose, B. K.: Power Electronics and AC Drives (1996). Prentice-Hall , Englewood Cliffs, New Jersey 07632, pp. 264-291.

[4] Ortega, R., Loria, A., Nicklasson, P., Sira – Ramirez, H. (1998). Passivity – Based Control of Euler – Lagrange Systems. Springer – Verlag, London, Berlin, Heidelberg.

[5] Ong, Ch. M. (1998). Dynamic Simulation of Electric Machinery. Prentice Hall, New York.

[6] Novotny, D. W., Lipo, T. A. (1996). Vector Control and Dynamics of AC Drives. Oxford University Press, New York.

[7] Pinto, J.O., Bose, B.K., da Silva, L. E. Borges (2001). A Stator – Flux – Oriented Vector – Controlled Induction Motor Drive With Space – Vector PWM and Flux – Vector Synthesis by Neural Networks. IEEE Transactions on Industry Applications, 37: 1308–1318.

[8] Keerthipala, W.L., Duggal, B.R., Chun, M.H. (1996). Implementation of Field – Oriented Control of Induction Motors using Neural Networks Observers. In: Proc. IEEE International Conference on Neural Networks, 3: 1795 – 1800.

[9] Ludtke, I., Jayne, M.G. (1995). Direct Torque Control of Induction Motors. In: IEEE Colloquium on Vector Control and Direct Torque Control of Induction Motors, London, U.K.

[10] Cabrera, L.A., Elbalak, M.E., Zinder, D.S. (1997). Learning Techniques to Train Neural Networks as a State Selector for Inverter Fed Induction Machines Using Direct Torque Control. IEEE Transactions on Power Electronics, 12:788 – 799.

[11] Orille, A. L., Sowilam, G. M. A. (1999). Application of Neural Networks for Direct Torque Control, Computers and Industrial Engineering, 37:391-394.

[12] Cabrera, L.A., Elbalak, M.E., Husaim, I. (1997). Tuning the Stators Resistance of Induction Motors Using Artificial Neural Networks. IEEE Transactions on Power Electronics, 12:779–787.

[13] Shi, K.L., Chan, T.F., Wong, Y.K., Ho, S.L. (2001). Direct Self Control of Induction Motor Based on Neural Network. IEEE Transactions on Industry Applications, 37:1290–1298.

[14] Simoes, M. G., Bose, B. K. (1995). Neural Network Based Estimation of Feedback Signals for a Vector Controlled Induction Motor Drive. IEEE Transactions on Industry Applications, 31:620–629.

[15] Ba – Razzouk, A., Cheriti, A., Olivier, G., Sicard, P. (1997). Field – Oriented Control of Induction Motors Using Neural – Network Decouplers. IEEE Transactions on Power Electronics, 12:752-763.

[16] Hagan, M. T., Menhaj, M. B. (1994). Training Feedforward Networks with the Marquardt Algorithm. IEEE Transactions on Neural Networks, 5:989-993.

[17] Demuth, H., Beale, M. (1992-2002). Neural Network Toolbox User's Guide, version 4, The Math Works, Inc. COPYRIGHT.